Turbulent Fracture Surfaces: A Footprint of Damage Percolation?

Stéphane Vernède,[1] Laurent Ponson,[2,*] and Jean-Philippe Bouchaud[3]
[1]Tortoise Analytics, 75005 Paris, France
[2]Institut Jean le Rond d'Alembert (UMR 7190), CNRS-Université Pierre et Marie Curie, 75005 Paris, France
[3]Capital Fund Management, 23 rue de l'Université, 75007 Paris, France

(Received 28 December 2014; revised manuscript received 6 March 2015; published 29 May 2015)

We show that a length scale ξ can be extracted from the spatial correlations of the "steep cliffs" that appear on a fracture surface. Above ξ, the slope amplitudes are uncorrelated and the fracture surface is monoaffine. Below ξ, long-range spatial correlations lead to a multifractal behavior of the surface, reminiscent of turbulent flows. Our results support a unifying conjecture for the geometry of fracture surfaces: for scales larger than ξ, the surface is the trace left by an elastic line propagating in a random medium, while for scales smaller than ξ, the highly correlated patterns on the surface result from the merging of interacting damage cavities.

DOI: 10.1103/PhysRevLett.114.215501 PACS numbers: 62.20.mm, 61.43.Hv, 64.60.av, 74.40.Gh

After thirty years of research, it is now well established that fracture surfaces exhibit robust universal fractal statistical properties, first reported in Ref. [1] and recently reviewed in Ref. [2]. Yet, identifying the physical mechanisms that lead to such fractal structures is still an open problem [3]. The most commonly used approach to characterize the roughness of fractal cracks is to study the scaling of the off-plane height variation δh of the fracture surface with the observation scale δr. The variance of this distribution shows a scaling law $\langle \delta h^2 \rangle \sim \delta r^{2\zeta}$ where ζ is the so-called roughness exponent. For purely brittle failure, the roughness exponent is reported to be $\zeta \approx 0.45$ [4,5] whereas for materials that undergo damage during failure $\zeta \approx 0.75$ [6,7]. It has been conjectured that these exponents are the signature of the fracture mechanism above and below the size of the process zone [8]. However, standard methods for extracting roughness exponents are not able to elicit the differences between the fracture mechanisms in the two regimes.

Here, we propose a different approach for characterizing crack roughness statistics by focusing on the local slopes of the fracture surfaces and their spatial correlations. This allows us to identify unambiguously two scaling regimes: above some length scale ξ, the slope amplitudes are uncorrelated and the fracture surface displays a monoaffine Gaussian behavior with a roughness exponent of $\zeta \approx 0.45$. Below ξ, long-range spatial correlations do appear and lead to a multifractal behavior of the surface. Our findings show that the presence of two distinct regimes of roughness first reported in Refs. [9,10] is a generic feature of fracture surfaces and is reminiscent of the brittle mode of failure that takes place at large scales and of the damage mechanisms present in the tip vicinity. In addition, it reveals the subtle organization of crack roughness at small length scales $\delta x < \xi$, reminiscent of the phenomenology of turbulent flows [11,12]. In particular, we relate quantitatively the multifractal spectrum measured at these length scales to the spatial correlations of the local slopes, and show that the largest slopes organize into a network of lines or "steep cliffs" that exhibit universal statistics. This new approach to the characterisation of fracture surfaces brings insights into the microscopic mechanisms at play during material failure, and in particular into the mechanism of damage percolation taking place at the tip of cracks. It also paves the way to a postmortem measurement of the size of the crack tip damaged zone, as a promising tool to infer material toughness from the statistical analysis of fracture surfaces.

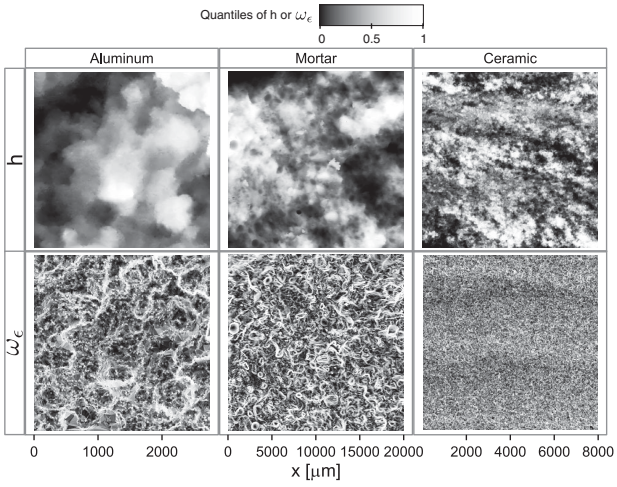

FIG. 1. Maps of h and ω_ϵ for the three materials studied. Top: the height h of the measured fracture surface. Bottom: transformation providing the field ω_ϵ of local slopes computed at a scale ϵ. In both cases, the quantiles of the distribution are represented by a gray hue, the largest values being represented by the lightest hue. ω_ϵ is computed at the scales $\epsilon = 3$, 50, and 8 μm for the aluminum, mortar, and ceramics fracture surfaces, respectively.

For this work, we have selected three sample materials that show a wide range of fracture behavior, namely an aluminum alloy, a mortar, and a sintered glass beads ceramic. The aluminum alloy specimens are aluminum 4 wt% copper broken under uniaxial mode I tension at 620 °C, in a semi-solid state [13]. The fracture surfaces are observed with a scanning electron microscope at two tilt angles and the elevation map is produced from a cross-correlation surface reconstruction technique. The mortar fracture surface is obtained by applying four points bending under controlled displacement conditions to a notched beam [9]. The topography of the fracture surfaces is recorded using an optical profilometer. The sintered glass beads ceramic fracture surfaces are obtained with a tapered double cantilever beam broken at a constant opening rate [5]. The roughness of the fractured specimen is measured using a mechanical stylus profilometer. Those fracture surfaces are described by their height field $h(\mathbf{x})$, a function of a two-dimensional in-plane vector $\mathbf{x}$, that is represented in a gray scale in the top panels of Fig. 1 for each material.

A first natural step in the characterization of the roughness statistics is to compute the distribution of height fluctuations at different scales. For a given increment $\delta\mathbf{x}$ of the coordinates in the average fracture plane, we note $p(\delta h|\delta\mathbf{x})$, the probability distribution of a height increment $\delta h = h(\mathbf{x}) - h(\mathbf{x}+\delta\mathbf{x})$, where the sampling of the distribution is done on all admissible coordinates $\mathbf{x}$. We also note $p(\delta h|\delta r)$, the distribution of δh where the sampling is done on all admissible $\mathbf{x}$ and $\delta\mathbf{x}$ such that $|\delta\mathbf{x}| = \delta r$. The distribution $p(\delta h|\delta r)$ at different δr is shown in a semi-logarithmic scale in Fig. 2 for the aluminum, mortar, and ceramic fracture surface. In this semilogarithmic representation, the parabolic shape of the distribution obtained for large values of δr reveals Gaussian statistics. This contrasts with the distributions observed for smaller values of δr that display fat tails. This drastic change in the shape of the distribution demonstrates that a single exponent is insufficient to describe the variations of the roughness properties with the scale of observation. Fat tail statistics also suggest the presence of over-represented large height variations over small in-plane distances that we would like to analyze further.

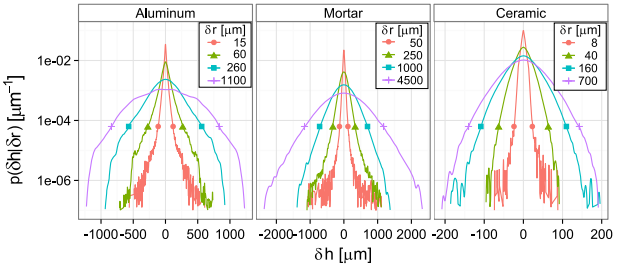

FIG. 2 (color online). Distribution of height fluctuations $p(\delta h|\delta r)$ at various scales δr for the three samples considered.

To investigate the spatial distribution of these steep "cliffs," we introduce the quantity $\omega_\epsilon(\mathbf{x})$ that measures the intensity of the local height variations of the fracture surface on a scale ϵ:

$$\omega_\epsilon(\mathbf{x}) = \frac{1}{2}\log\left(\langle \delta h(\mathbf{x},\delta\mathbf{x})^2\rangle_{|\delta\mathbf{x}|=\epsilon}\right) - \Omega_\epsilon. \quad (1)$$

$\delta h(\mathbf{x},\delta\mathbf{x}) = h(\mathbf{x}+\delta\mathbf{x}) - h(\mathbf{x})$ is the local slope of the surface in the direction $\delta\mathbf{x}$, and Ω_ϵ is chosen such that the average of $\omega_\epsilon(\mathbf{x})$ over all $\mathbf{x}$ is zero. Note that the average of the slopes is done over a circle of radius ϵ. This new field $\omega_\epsilon(\mathbf{x})$ has several interesting properties, like isotropy and robustness to measurement artifacts. The maps of ω_ϵ calculated from the off-plane height maps h shown in Fig. 1 are represented in the lower panels in the same figure. Strikingly, the largest values of ω_ϵ (lighter gray), corresponding to the steep cliffs that populate the tails of the distribution $p(\delta h|\delta r)$, are spatially correlated and form a network of rough lines for the aluminum and the mortar fracture surfaces. For the ceramic fracture surface, smaller patterns are visible.

The visually correlated patterns in Fig. 1 can be quantified by computing the spatial correlations of ω_ϵ, which we further average over all directions [14], i.e., $C_\epsilon(\delta r) = \langle \omega_\epsilon(\mathbf{x})\omega_\epsilon(\mathbf{x}+\delta\mathbf{x})\rangle_{\mathbf{x},|\delta\mathbf{x}|=\delta r}$. This quantity is shown in Fig. 3 as a function of the distance δr for different observation scales ϵ; $C_\epsilon(\delta r)$ is independent of ϵ whenever $\epsilon \ll \delta r$. For the three materials considered, we clearly observe two regimes. At small δr, ω_ϵ shows strong spatial correlations, which decay logarithmically with distance, i.e., $C_\epsilon(\delta r) \sim -\lambda\log(\delta r/\xi)$, and extrapolates to zero for $\delta r = \xi$. For larger distances, these correlations are zero within statistical noise. Both λ and ξ are found to be, to a good approximation, independent of ϵ provided $\epsilon \ll \xi$. Note that λ is a dimensionless number and its value is empirically found to be quite similar for the three materials at hand: 0.21 ± 0.02 (aluminum), 0.15 ± 0.03 (mortar), and 0.15 ± 0.06 (ceramics). The crossover length ξ is found to be 170 ± 12, 430 ± 35, and 50 ± 9 μm, respectively. Note that the ratio of ξ to the total map size is 0.06, 0.02,

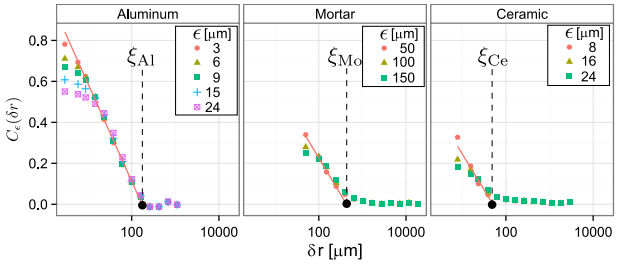

FIG. 3 (color online). Spatial correlations of ω_ϵ for the three materials considered. The correlations are represented for ω_ϵ computed at different scales ϵ. The cutoff length ξ is represented for each case.

and 0.006, respectively. These last values confirm the visual impression conveyed by Fig. 1 where large correlated patterns are observed for aluminum, smaller patterns for mortar, and even smaller ones for ceramics.

In order to characterize further the two regimes, we now compute the multifractal spectrum of the height fluctuations, defined through $\langle|\delta h(\mathbf{x},\delta\mathbf{x})|^q\rangle_{\mathbf{x},|\delta\mathbf{x}|=\delta r} \sim \delta r^{\zeta_q}$ for the two ranges of length scales $\delta r < \xi$ and $\delta r > \xi$. Note that the standard roughness exponent ζ corresponds to $q = 2$, and $\zeta \equiv \zeta_2/2$. For $\delta r > \xi$, we observe that ζ_q/q is fairly independent of q with a value around 0.45 (see the rhs of Fig. 4). This corresponds to a monoaffine behavior, i.e. a scaling that preserves the shape of the full distribution $p(\delta h|\delta r)$ of height fluctuations. This is consistent with the observation of a conserved Gaussian distribution at large scales (see Fig. 2), and is in agreement with previous findings [10,16,17]. The monoaffine behavior is very clear for the mortar and the ceramic fracture surface. For the aluminum fracture surface, some residual variations of ζ_q/q with q are observed; this behavior may be due to the rather limited extension of the large scale regime $\delta r > \xi$.

For $\delta r < \xi$, on the other hand, we do observe a significant variation of ζ_q/q with q, as reported in former studies [18,19]. This multiaffine behavior can in fact be traced back to the logarithmic decay of the spatial correlations $C_\epsilon(\delta r)$ of the slopes discussed above. Indeed, assuming that ω_ϵ is a Gaussian field, and that the local slope can be written as $\delta h(\mathbf{x},\delta\mathbf{x}) = e^{\omega_\epsilon(\mathbf{x})} s_\epsilon(\mathbf{x})$ with $|\delta\mathbf{x}| = \epsilon$, and $s_\epsilon(\mathbf{x})$ is a long ranged correlated random variable with unit variance and $\langle s_\epsilon(\mathbf{x}) s_\epsilon(\mathbf{x}+\delta\mathbf{y})\rangle_{\mathbf{x},|\delta\mathbf{y}|=\delta r} \sim |\delta r|^{-\gamma}$, one derives, adapting the calculations of Ref. [20] (see the Supplemental Material [21])

$$\zeta_q = q\left(H - (q-1)\frac{\lambda}{2}\right) \quad \text{with} \quad H \equiv \zeta_1 = \left(1 - \frac{\gamma}{2}\right), \tag{2}$$

where λ is the slope of the logarithmic correlation defined above. As seen in the lhs of Fig. 4, where the predictions of Eq. (2) are represented by straight lines, the slope of the multifractal spectrum is indeed well captured by this simple model. We have measured the exponent γ independently, from the spatial correlations of the signs of the local slopes in a given direction, with good agreement with the direct estimate of H, in particular for aluminum where the scaling region is large. We therefore claim that fracture surfaces are, on short length scales, bidimensional realizations of multifractal, persistent Brownian motions. Whereas natural realizations of multifractal Brownian motions with $H \leq 1/2$ have been reported in turbulent flows ($H \approx 1/3$) [11] and in financial time series ($H \approx 1/2$) [20], it is to our knowledge the first time that a multifractal signal with $H > 1/2$ has been observed. The curvature of the multifractal spectrum seen in Fig. 4 cannot be captured by Eq. (2). This can be traced back to the assumption that ω_ϵ is a Gaussian field. Introducing nontrivial higher order correlations of ω_ϵ that also decay logarithmically would add higher order contributions to ζ_q. However, these higher order correlations are difficult to measure and we lack statistics to test the model beyond the second order correlations reported here [22].

To characterize further the spatial organization of the steepest regions and its robustness towards material specificity, we study the geometrical properties of the clusters formed by the largest values of ω_ϵ, i.e. the ridge of the cliffs. The field ω_ϵ is thresholded in order to keep only a fraction p_{th}. These extreme events organize in a network of disconnected clusters, as suggested by the bottom of Fig. 1 (see also Fig. 1 of the Supplemental Material [21]). The extension ℓ of each cluster can be defined using either its extension along the horizontal or vertical axis, or its radius of gyration R_g. These three quantities are found to follow the same scaling $S \sim \ell^D$ with the number of pixels (or area) S contained by the cluster, suggesting that these clusters have a fractal geometry with dimension $D \approx 1.70 \pm 0.15$, again independently of the material considered (see the Supplemental Material [21]). We show in Fig. 5 the distribution of cluster sizes for different values of the

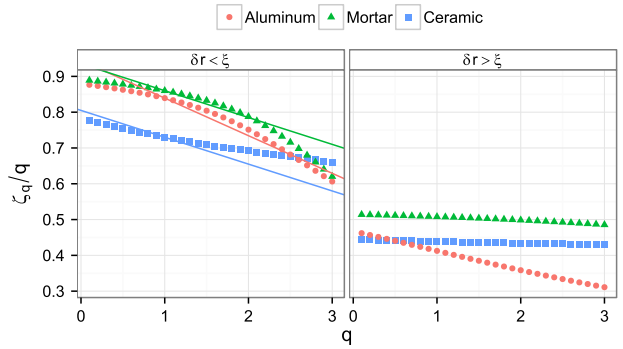

FIG. 4 (color online). Multifractal spectrum of the fracture surfaces. The spectrum is computed both below (left) and above ξ (right). The spectrum predicted for $\delta r < \xi$ by the multifractal model of Eq. (2) is represented by a straight line.

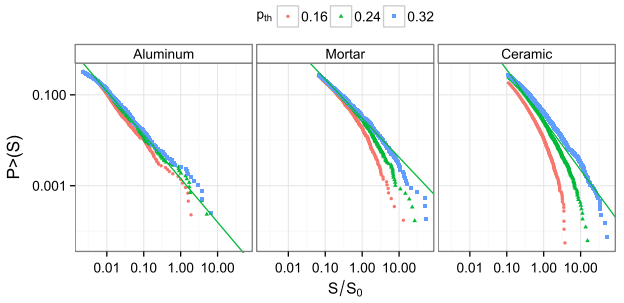

FIG. 5 (color online). Cumulative distribution function $P_>(S)$ of cluster size for different thresholds p_{th}. The normalization factor S_0 is the average size of a cluster with a gyration radius equal to ξ.

TABLE I. Statistical parameters extracted from the fracture surfaces (see text for details).

	λ	D	τ	ξ
Aluminum	0.21 ± 0.02	1.68 ± 0.10	0.96 ± 0.1	170 ± 12 μm
Mortar	0.15 ± 0.03	1.73 ± 0.08	0.86 ± 0.1	430 ± 35 μm
Ceramics	0.15 ± 0.06	1.74 ± 0.12	1.1 ± 0.2	50 ± 9 μm

threshold p_{th}. For clusters of scales smaller than ξ, we observe a power law for the cumulative distribution function $P_{>}(S) \sim S^{-\tau}$ with exponent $\tau \approx 1.0 \pm 0.2$ for all three materials [23]. This means that not only the roughness exponent ζ but at least three other quantities describing the statistics of fracture surfaces are universal in the small δr regime: λ, which describes the spatial correlations of the amplitude of slopes and the multifractal spectrum, D, which is the fractal dimension of the ridge of the cliffs on the fracture surface, and τ, which characterizes the cluster size distribution (see Table I for a comparison of their values from one material to another). This extended universality is important for at least two reasons: (i) it provides additional support for the conjecture that the statistics of fracture surfaces is universal, suggesting a common underlying roughening mechanism, and (ii) it provides important further constraints that must be abided by in any theory attempting to explain the universal value of the roughness exponent $\zeta \approx 0.75$ [6,7].

What is the physical interpretation of these observations? We believe that the presence of spatially correlated steep cliffs on short length scales $\delta r < \xi$ is a strong indication that at these scales, fracture proceeds through the nucleation and coalescence of microcracks or damage cavities, as previously conjectured [24–27]. As elaborated in the context an estimate of planar cracks [28,29], the scale ξ therefore provides the extent ℓ_{pz} of the fracture process zone [30]. It also reflects the material toughness, since $K_{\mathrm{Ic}} \simeq \sigma_c \sqrt{\ell_{\mathrm{pz}}}$, where σ_c is the typical failure stress under tension [31]. Our methodology based on the correlation of slopes measured on the fracture surfaces therefore paves the way for a postmortem characterization of material toughness from the statistical analysis of their fragments [32].

Although this is still an open theoretical issue, the percolation of power law distributed microcracks should provide a rationale for the value of the small scale roughness exponent $\zeta \approx 0.75$. Discontinuities along the fracture surface are the stigma of these coalescing cavities [33] and this picture should be made compatible with values of the new, universal statistical indicators reported here, namely λ, D, and τ. Only on large length scales $\delta r > \xi$ does the notion of a continuous fracture line make sense. Continuum fracture mechanics based models describing crack fronts as an elastic interface driven in a random medium [8,17,26,34–38] predict monoaffine Gaussian fracture surfaces with $\zeta \approx 0.4$ [8,17], indeed compatible with our findings.

We thank D. Bonamy, E. Bouchaud, Y. Cao, A. Hansen, J.-F. Muzy, and S. Morel for fruitful discussions. The support from the European Union through the Marie Curie Integration Grant "ToughBridge" and from the city of Paris through the Emergence Program is gratefully acknowledged (L. P.).

*Corresponding author.
laurent.ponson@upmc.fr

[1] B. B. Mandelbrot, D. E. Passoja, and A. J. Paullay, Nature (London) **308**, 721 (1984).
[2] D. Bonamy and E. Bouchaud, Phys. Rep. **498**, 1 (2011).
[3] M. J. Alava, P. K. Nukala, and S. Zapperi, Adv. Phys. **55**, 349 (2006).
[4] J. M. Boffa, C. Allain, and J. P. Hulin, Eur. Phys. J. Appl. Phys. **2**, 281 (1998).
[5] L. Ponson, H. Auradou, P. Vié, and J. P. Hulin, Phys. Rev. Lett. **97**, 125 501 (2006).
[6] E. Bouchaud, G. Lapasset, and J. Planès, Europhys. Lett. **13**, 73 (1990).
[7] K. J. Måløy, A. Hansen, E. L. Hinrichsen, and S. Roux, Phys. Rev. Lett. **68**, 213 (1992).
[8] D. Bonamy, L. Ponson, S. Prades, E. Bouchaud, and C. Guillot, Phys. Rev. Lett. **97**, 135 504 (2006).
[9] S. Morel, D. Bonamy, L. Ponson, and E. Bouchaud, Phys. Rev. E **78**, 016 112 (2008).
[10] S. Santucci, K. J. Måløy, A. Delaplace, J. Mathiesen, A. Hansen, J. Ø. H. Bakke, J. Schmittbuhl, L. Vanel, and P. Ray, Phys. Rev. E **75**, 016 104 (2007).
[11] U. Frisch, *Turbulence: The Legacy of A. Kolmogorov* (Cambridge University Press, Cambridge, England, 1997).
[12] J. Krug, Phys. Rev. Lett. **72**, 2907 (1994).
[13] S. Vernède, Ph.D. thesis, EPFL, Lausanne, 2007.
[14] We assume, for simplicity, that fracture surfaces are statistically isotropic. This is only approximately correct, since one expects the roughness in the direction parallel to the crack propagation and perpendicular to it to be different [15]. The extension of our results to a multifractal anisotropic Family-Vicsek scaling is left for a future study.
[15] L. Ponson, D. Bonamy, and E. Bouchaud, Phys. Rev. Lett. **96**, 035 506 (2006).
[16] L. Ponson, H. Auradou, M. Pessel, V. Lazarus, and J.-P. Hulin, Phys. Rev. E **76**, 036 108 (2007).
[17] L. Ponson, Ann. Phys. (Paris) **32**, 1 (2007).
[18] E. Bouchbinder, I. Procaccia, S. Santucci, and L. Vanel, Phys. Rev. Lett. **96**, 055 509 (2006).
[19] E. Bouchaud, D. Boivin, J.-L. Pouchou, D. Bonamy, B. Poon, and G. Ravichandran, Europhys. Lett. **83**, 66006 (2008).
[20] J. F. Muzy, J. Delour, and E. Bacry, Eur. Phys. J. B **17**, 537 (2000).
[21] See Supplemental Material at http://link.aps.org/supplemental/10.1103/PhysRevLett.114.215501 for the calculation of the multifractal spectrum of long-range correlated processes and the characterization of the fractal geometry of the clusters of extreme events.
[22] Attempts to measure the third order correlations of the ω_ϵ field however lead to the correct sign of the curvature of ζ_q/q.

[23] It is interesting to note that the clusters of a log-correlated Gaussian field in two dimensions have been studied in full details in D. Bernard, G. Boffetta, A. Celani, and G. Falkovich, Phys. Rev. Lett. **98**, 024501 (2007), where the values $D = 15/8$ and $\tau = 16/15$ are predicted. These values are indeed close to the ones observed here for the ω field clusters. The discrepancies may have several causes, in particular the anisotropy of the surfaces and the non-Gaussian nature of ω—see Refs. [14,21].
[24] F. Paun and E. Bouchaud, Int. J. Fract. **121**, 43 (2003).
[25] K. Ravi-Chandar and B. Yang, J. Mech. Phys. Solids **45**, 535 (1997).
[26] E. Bouchaud, J. P. Bouchaud, D. S. Fisher, S. Ramanathan, and J. R. Rice, J. Mech. Phys. Solids **50**, 1703 (2002).
[27] A. Hansen and J. Schmittbuhl, Phys. Rev. Lett. **90**, 045 504 (2003).
[28] S. Santucci, M. Grob, R. Toussaint, J. Schmittbuhl, A. Hansen, and K. J. Måløy, Europhys. Lett. **92**, 44 001 (2010).
[29] K. S. Gjerden, A. Stormo, and A. Hansen, Phys. Rev. Lett. **111**, 135 502 (2013).
[30] This result can be tested using Barrenblat's formula $\ell_{\mathrm{pz}} = \pi/8(K_{Ic}/\sigma_c)^2$, where K_{Ic} is the material toughness and σ_c its tensile strength [31]. Values reported in Ref. [17] for glass ceramics lead to $\ell_{\mathrm{pz}} = 40$ μm close to the value $\xi = 50$ μm while the application of this formula to Portland based concretes gives $\ell_{\mathrm{pz}} = 1.7$ mm, which is larger than, but of the same order as of magnitude $\xi = 430$ μm.
[31] G. I. Barenblatt, Adv. Appl. Mech. **7**, 55 (1962).
[32] S. Vernède and L. Ponson, French Patent Application No. 1459525. For more information, see www.tortoise.io.
[33] C. Guerra, J. Scheibert, D. Bonamy, and D. Dalmas, Proc. Natl. Acad. Sci. U.S.A. **109**, 390 (2012).
[34] H. Gao and J. R. Rice, J. Appl. Mech. **56**, 828 (1989).
[35] J. P. Bouchaud, E. Bouchaud, G. Lapasset, and J. Planès, Phys. Rev. Lett. **71**, 2240 (1993).
[36] J. Schmittbuhl, S. Roux, J. P. Vilotte, and K. J. Måløy, Phys. Rev. Lett. **74**, 1787 (1995).
[37] S. Ramanathan, D. Ertas, and D. S. Fisher, Phys. Rev. Lett. **79**, 873 (1997).
[38] D. Bonamy, S. Santucci, and L. Ponson, Phys. Rev. Lett. **101**, 045501 (2008).

Turbulent fracture surfaces: A footprint of damage percolation? Supplementary Material

Stéphane Vernède,[1] Laurent Ponson,[2] and Jean-Philippe Bouchaud[3]

[1] *Tortoise Analytics, 75005 Paris, France*
[2] *Institut Jean le Rond d'Alembert (UMR 7190), CNRS - Université Pierre et Marie Curie, 75005 Paris, France*
[3] *Capital Fund Management, 23 rue de l'Université, 75007 Paris, France*

GENERALIZATION OF THE BACRY-DELOUR-MUZY ANALYSIS FOR LONG-RANGE CORRELATED PROCESSES

For simplicity, we only consider here one dimensional profiles $h(x)$. We write the slope δh on scale ϵ as $\delta h(x) = s(x)e^{\omega(x)}$, where $s(x)$ has long-range correlations described by the exponent γ and $\omega(x)$ is a Gaussian field with logarithmic corrections with slope $-\lambda$. Then, by definition,

$$h(x) - h(0) = \sum_{i=1}^{x/\epsilon} \delta h(x_i), \qquad x_i := i\epsilon. \tag{1}$$

We want to compute the various moments of $h(x) - h(0)$. For even values of $q = 2m$, and assuming for simplicity that $s(x)$ is Gaussian that allows one to use Wick's theorem, one has:

$$\langle (h(x) - h(0))^q \rangle = C_{2m}^m \sum_{i_1,\ldots,i_{2m}} \langle s(x_1)s(x_2)\rangle \ldots \langle s(x_{2m-1})s(x_{2m})\rangle \langle e^{\sum_{\alpha=1}^{2m} \omega(x_\alpha)}\rangle. \tag{2}$$

Now, since the ω's are also Gaussian with a logarithmic correlation function, one has:

$$\langle e^{\sum_{\alpha=1}^{2m} \omega(x_\alpha)}\rangle = C e^{-\frac{\lambda}{2}\sum_{\alpha\neq\beta=1}^{2m} \ln|x_\alpha - x_\beta|}, \tag{3}$$

where C is a constant that accounts for the diagonal terms $\alpha = \beta$, that plays no role in the following.

Let us first consider the Bacry-Delour-Muzy (BDM) case where $s(x)$ has only short range correlation, say even purely local: $\langle s(x_1)s(x_2)\rangle = \delta_{x_1,x_2}$. This local contribution will always exist, even in the long-range case, and will eventually have to be compared to the latter contribution in order to determine the dominant one. In the BDM case, this imposes $x_{2j+1} = x_{2j+2}$, and therefore:

$$e^{-\frac{\lambda}{2}\sum_{\alpha\neq\beta=1}^{2m} \ln|x_\alpha - x_\beta|} \propto e^{-2\lambda\sum_{j\neq k=1}^{m} \ln|x_{2j} - x_{2k}|}. \tag{4}$$

Hence, approximating discrete sums by integrals in the limit $\epsilon \to 0$, one has:

$$\langle (h(x) - h(0))^q \rangle \propto \int_0^x \ldots \int_0^x \mathrm{d}x_2 \ldots \mathrm{d}x_{2m} \prod_{j\neq k=1}^{m} |x_{2j} - x_{2k}|^{-2\lambda}. \tag{5}$$

Setting $x_{2j} = x\,u_{2j}$, one finds by simple power-counting (which is correct provided the resulting integral on u's converges, i.e. when $\zeta_q > 0$; see [1]):

$$\langle (h(x) - h(0))^q \rangle \propto x^m \times x^{2\lambda m(m-1)} \equiv x^{\zeta_q}, \tag{6}$$

or $\zeta_q = q/2(1 - \lambda(q-2))$, which is precisely the BDM result [1].

Now, if one assumes that for large distances $\langle s(x_1)s(x_2)\rangle \propto |x_1 - x_2|^{-\gamma}$, the corresponding contribution to the q-th moment of $h(x) - h(0)$ reads:

$$\langle (h(x) - h(0))^q \rangle \propto \tag{7}$$

$$\int_0^x \ldots \int_0^x \mathrm{d}x_1\mathrm{d}x_2 \ldots \mathrm{d}x_q \prod_{\ell=0,m-1} |x_{2\ell+1} - x_{2\ell}|^{-\gamma} \prod_{j\neq k=1}^{q} |x_j - x_k|^{-\lambda/2} \tag{8}$$

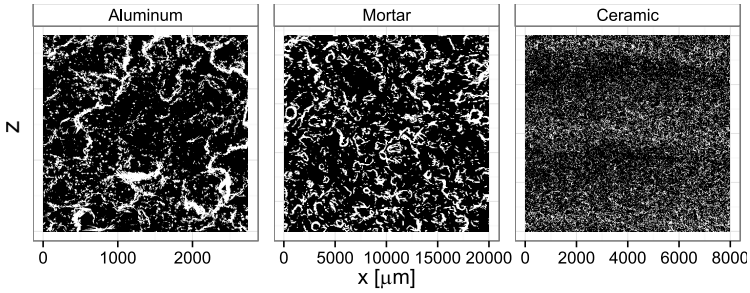

FIG. 1: Clusters formed by the largest values of ω_ϵ for a threshold $p_{\rm th} = 0.2$ for the three materials studied.

Power-counting now leads to:

$$\zeta_q = q - q\frac{\gamma}{2} - q(q-1)\frac{\lambda}{2} \equiv q(H - (q-1)\frac{\lambda}{2}), \qquad H = 1 - \frac{\gamma}{2}, \tag{9}$$

as given in the text. However, one has to compare this last contribution to the BMD one, leading to the following inequality:

$$q(1 - \frac{\gamma}{2} - (q-1)\frac{\lambda}{2}) \geq \frac{q}{2}(1 - \lambda(q-2)) \longrightarrow \gamma < 1 - \lambda, \tag{10}$$

independently of q. This last condition is well satisfied in practice, since $\gamma \approx 0.4 - 0.5$ and $\lambda \approx 0.15 - 0.2$.

STATISTICAL CHARACTERIZATION OF CLUSTERS FORMED BY THE LARGEST VALUE OF ω_ϵ

The distributions of height fluctuations in the materials investigated do not follow a mono-affine Gaussian behavior at small scale because of the extended fat tails of $p(\delta h|\delta r)$. As the observation scale δr is decreased, these tails indeed become more pronounced, resulting in the multi-affine behavior revealed by the spectrum ζ_q (see Fig. 4 of the main article). To proceed to a quantitative analysis of the spatial distribution of the steepest slopes that contribute to the distribution tails, we introduce $\omega_\epsilon(\mathbf{x})$ defined by Eq. (1) as a transformation of the original fracture map that allows for a straightforward localization of these extreme events (see Fig. S1). As the focus is put on these steepest slopes, the new maps $\omega_\epsilon(\mathbf{x})$ are thresholded, and the fraction $p_{\rm th}$ of the total number of pixels of the original map is conserved. We choose $p_{\rm th}$ in the range $0.05 - 0.32$. The position of the steepest slopes is represented on Fig. S1 for $p_{\rm th} = 0.20$ on the aluminum, mortar and ceramics fracture surfaces.

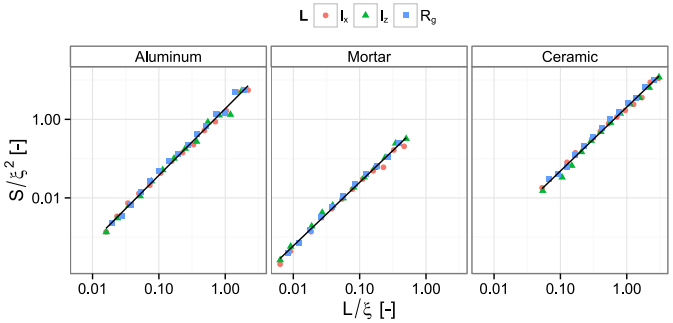

FIG. 2: Cluster surface as a function of its typical length scale ℓ for the three samples considered. The length ℓ is either the cluster radius of gyration $R_{\rm g}$, or its extension along the horizontal $\ell_{\rm x}$ and vertical axis $\ell_{\rm z}$. All lengths are normalized by the crossover length ξ.

The statistical characterization of the geometry of these clusters is now detailed. We investigate first the geometry of the isolated clusters. Figure S2 shows the variation of cluster area as a function of three typical length scales

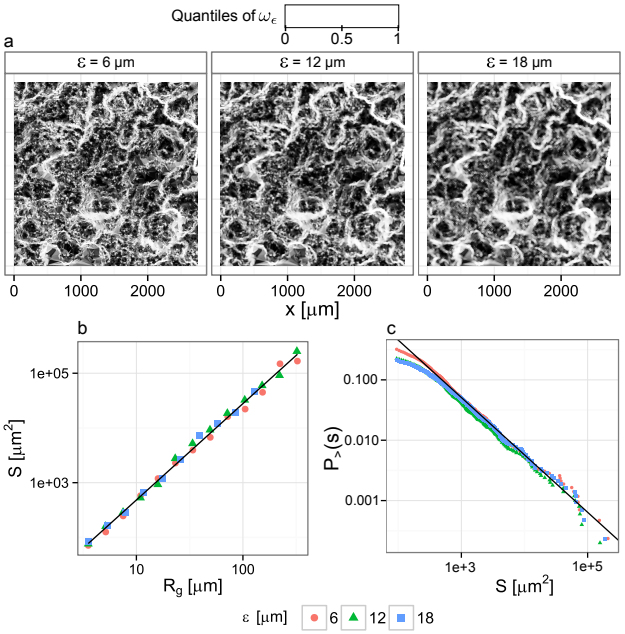

FIG. 3: Effect of the scale ϵ on the cluster properties for the aluminum fracture surface: (a) ω_ϵ field; (b) fractal geometry of the clusters; (c) cumulative distribution function $P_>(S)$ of cluster size

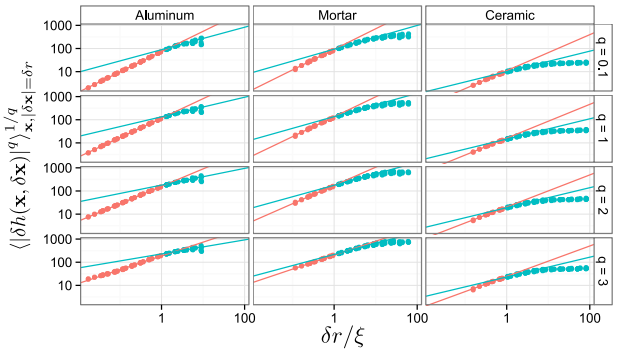

FIG. 4: Determination of the multifractal spectrum below and above ξ for the three samples at various values of q.

characterizing the cluster size, namely its extension ℓ_x along the propagation direction, its extension ℓ_z perpendicular to it and its radius of gyration R_g. These three quantities characterize equivalently the fractal geometry of the clusters since they all scale as $\sim S^D$, where the fractal dimension $D \simeq 1.7 \pm 0.15$ irrespective of the material considered. The cumulative distribution function $P_>(S)$ of cluster size are shown on Fig. 5 of the main article, and follow power laws with exponent $\tau \simeq 1 \pm 0.2$.

We investigate now the robustness of these findings towards our statistical procedure. The role of $p_{\rm th}$ on the cluster statistics is investigated on Fig. 5 of the main article, and does not show any noticeable effect. Similarly, we observe that $p_{\rm th}$ has a negligible effect on the cluster fractal dimension. The effect of the scale ϵ on the cluster statistical characterization is illustrated on Fig. S3 in the case of the aluminum fracture surface. The clusters display robust statistical properties independent of the length ϵ as long as one considers sufficiently large cluster sizes $R_g \gg \epsilon$.

DETERMINATION OF THE MULTIFRACTAL SPECTRUM BELOW AND ABOVE ξ

Figure 4 shows the relation $\langle|\delta h(\mathbf{x},\delta\mathbf{x})|^q\rangle_{\mathbf{x},|\delta\mathbf{x}|=\delta r} \sim \delta r^{\zeta_q}$ fitted for δr below and above ξ at various of q. This procedure is used to produce the multifractal spectrum in figure 4 of the main article.

[1] J. F. Muzy, J. Delour, and E. Bacry *Eur. Phys. J. B* **17**, 537 (2000).

Focus: Crack Patterns Resemble Fluid Turbulence

May 29, 2015 • *Physics* 8, 50

A statistical analysis of crack surfaces from three different materials reveals a deep connection with fluid turbulence and a potentially new approach to studying failed machine parts.

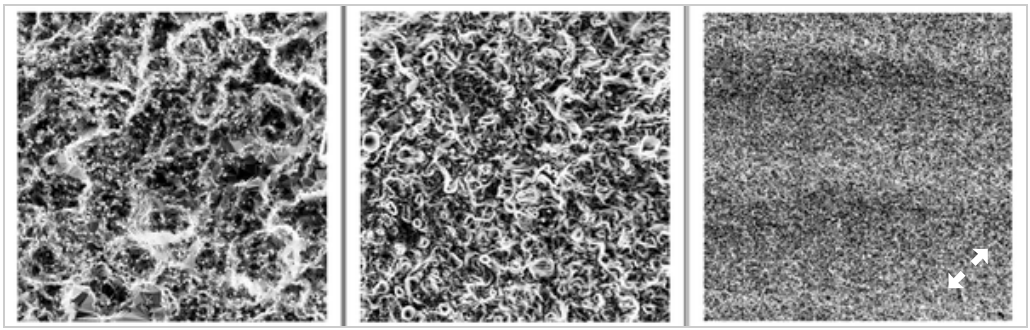

S. Vernède *et al.*, Phys. Rev. Lett. (2015)

Topography of a crack. Fracture surface images processed to highlight the steepest cliffs of (left to right) aluminum, mortar, and ceramic in frames that are 3, 20, and 8 mm wide, respectively. The steepest cliffs are white and appear to have a pattern rather than being entirely random. **Show less**

Physicists have found a surprising link between fluid turbulence and the complex surfaces created during the fracture of a solid material. Mathematical analysis of fractured surfaces in materials with widely different properties confirms a theoretical conjecture made some 20 years ago about the fracture process on microscopic scales. The work could lead to new ways of determining a material's mechanical properties based on scans of its fracture surfaces.

The fracture of a brick or piece of metal creates rough surfaces with so-called fractal or self-similar structures. Small portions of the surface, if magnified, look identical to larger portions. This pattern of self-similarity is also universal, arising during the fracture of essentially any solid material.

Researchers understand the origin of this universality, at least on long length scales, where fracture patterns reflect the universal way that a crack propagates as it navigates around material inhomogeneities. On small scales, however, researchers don't know why the resulting structures don't vary significantly from one material to another. Jean-Philippe Bouchaud of Capital Fund Management in Paris and his colleagues now argue that the character of fractured surfaces on small scales reflects the way microscopic cracks grow and then rapidly coalesce in the material. This process happens in an identical way even in different materials, in much the same way that all turbulent fluids behave identically.

The researchers fractured three very different materials—aluminum, mortar, and ceramic. Using various imaging methods such as electron microscopy, they created maps of the irregular fracture surfaces and analyzed them statistically. This raw data showed that, over short distances, the surfaces didn't go up and down in a gentle, continuous way, but were instead characterized by a preponderance of steep cliffs.

The team then analyzed this raw data further, looking at how the steepest of these cliffs were distributed spatially over the surface. The analysis showed that for each material, the cliffs were nested in a highly organized pattern known as a multifractal, which is a mixture of many fractals. A fractal pattern is always characterized by a number called its fractal dimension; a multifractal is a mathematical combination of fractals with a range of fractal dimensions.

Observing multifractal properties is significant, the researchers suggest, because multifractals have previously been seen mainly in two other settings—fluid turbulence and financial time series. Further mathematical analysis of the cliff distribution showed that at least three distinct numbers characterizing the pattern were virtually identical for the three different materials, suggesting some deep uniformity in the fracture process that creates these cliffs.

This universality may point to a process, suggested by physicists almost 20 years ago [**1**], in which fracture proceeds in a material through the creation of multiple microcracks, or "damage cavities," which recombine and coalesce rapidly as the crack propagates. "In the process," says Bouchaud, "voids get created and expand, deforming the material and creating more voids. Then when they coalesce, they leave behind these 'steep cliffs', or 'scars'." This process dissipates energy in the material and seems to happen the same way in every material. In fluid turbulence, instead of voids creating voids, it's large-scale eddies that produce eddies at smaller and smaller scales, until the smallest ones simply generate heat (dissipate energy). This turbulent "cascade" is similar in all fluids.

Other physicists are surprised by the strength of the apparent link to turbulence. “Some 20 years ago we had thought about an analogy between turbulence and rough surfaces on purely formal grounds,” says Joachim Krug of the University of Cologne in Germany. “But I wouldn’t have expected turbulence concepts to become useful for understanding the surfaces of real materials. I’m really intrigued.”

Aside from this fundamental understanding of fracture, Bouchaud and colleagues believe this work may also lead to new ways to characterize fractured surfaces. By looking at the patterns of steep cliffs, it should be possible to estimate a material’s ability to avoid fracturing under stress (toughness), says team member Stéphane Vernède of the Pierre and Marie Curie University in Paris. This procedure might be useful in the aftermath of air crashes or other accidents when investigators search for the root of a material failure.

This research is published in **Physical Review Letters**.

–Mark Buchanan

Mark Buchanan is a freelance science writer in Normandy, France. He writes a **blog on physics and finance**.

References

1. K. Ravi-Chandar and B. Yang, “On the Role of Microcracks in the Dynamic Fracture of Brittle Materials,” **J. Mech. Phys. Solids 45, 535 (1997)**

Subject Areas

Materials Science

Turbulent Fracture Surfaces: A Footprint of Damage Percolation?

Stéphane Vernède, Laurent Ponson, and Jean-Philippe Bouchaud

Phys. Rev. Lett. 114, 215501 (2015)

Published May 29, 2015